ACS OMEGA

http://pubs.acs.org/journal/acsodf

Article

Exploration of Basalt Glasses as High-Temperature Sensible Heat Storage Materials

Jianxun Liu,* Zhongchen Chang, Lianbo Wang, Jingwen Xu, Rao Kuang,* and Zhishen Wu*

Cite This: *ACS Omega* 2020, 5, 19236−19246

Read Online

ACCESS | Metrics & More | Article Recommendations

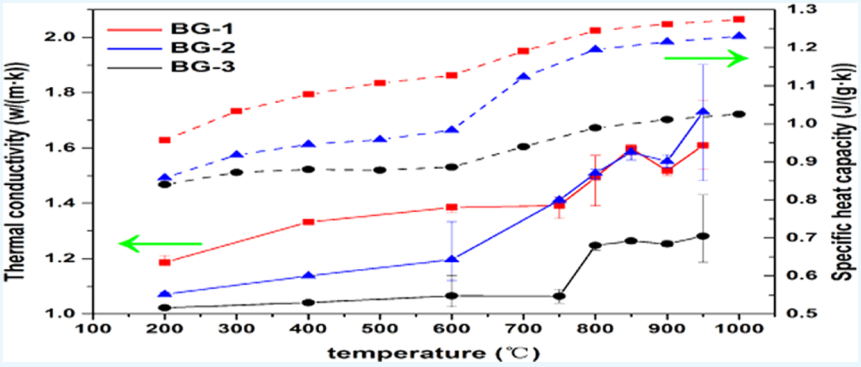

ABSTRACT: Thermal energy storage (TES) systems are a key technology that utilizes renewable energy and low-level thermal energy to ensure continuous and stable operation in concentrated solar power plants, family heating, and industrial waste heat recovery fields. It solves the intermittent problem of solar radiation and significantly improves energy efficiency and economic benefits. Three varieties of natural basalt ores have been selected, namely, intermediate, basic, and ultrabasic basalt, which have been prepared into basalt glasses by the melt-quenching method. The applicability of basalt glass to high-temperature heat storage applications is studied. In the present paper, the chemical composition and structure of basalt glasses have been determined. The effect of temperature and composition on key thermophysical properties such as density, heat capacity, thermal diffusion, thermal conductivity, and thermal expansion has been analyzed during a series of thermal cycles. It has been confirmed that basalt glass has extremely high heat storage performance and thermal stability, and its working temperature is as high as 1000 °C such that it can be used as a solar energy heat storage material.

1. INTRODUCTION

In recent years, due to the rapid development of global industrialization and the population growth, the demand for energy is growing. Nevertheless, the large-scale use of fossil fuels has not only triggered an energy crisis but also caused serious environmental pollution by greenhouse gas emissions such as carbon dioxide. Researchers from all over the world are committed to the research and development of renewable energy systems. Solar energy is the most abundant and clean energy on earth. The efficient collection and utilization of solar energy is the most important technology to solve the energy crisis and environmental problems, but the radiation of solar energy is intermittent, the energy cannot be output smoothly and effectively, and its application is limited in time and space.[1] Thermal energy storage (TES) systems have emerged as one of the most promising candidates for solving this issue, and thermal storage materials are the core elements of these systems.[2] A heat storage system can convert solar energy into heat energy and store it, then output the energy via a heat transfer medium when needed. It can adjust the balance between energy supply and demand, and it plays a crucial role in solar power plants and home heating.[3] Solar thermal power generation is the most appropriate and flexible way to generate electricity from renewable sources.[4] The heat storage materials are generally divided into three categories according to the form of storage, namely sensible heat, latent heat, and chemical heat storage materials. Sensible heat storage materials store and release energy through temperature change, which does not involve the phase change process;[5] typical materials include mineral rocks, concretes, water, oil, and molten salts.[4] Latent heat storage materials are based on the phase change (solid−liquid, solid−solid, etc.) of the substance, which can store and

Received: June 11, 2020
Accepted: July 16, 2020
Published: July 27, 2020

Table 1. Chemical Compositions of Basalt Glasses (mol %)

(mol %)	SiO_2	Al_2O_3	Fe_2O_3	CaO	MgO	TiO_2	K_2O	Na_2O	P_2O_5
BG-1	62.3	10.72	4.02	8.04	8.71	0.67	1.34	4.02	0.19
BG-2	57.41	9.21	7.09	12.05	7.8	2.83	0.71	2.84	0
BG-3	49.83	9.43	5.39	11.45	15.49	2.69	1.35	4.04	0.35

release energy during the phase change process, also known as phase change materials (PCMs).[6] There are various common PCMs such as calcium chloride hexahydrate, sodium acetate trihydrate, and organic alcohol.[7] Chemical heat storage materials, such as NH_3, ammonium hydrogen sulfate, and hydroxide,[8−10] realize the energy charging and discharging by making use of chemical heat during reversible chemical reactions. Among them, phase change heat storage materials are mainly organic and inorganic salts, which are expensive, corrosive to containers, poor in thermal stability, and low in working temperature. Although the chemical heat storage material has a large amount of heat storage, it has high requirements for equipment and technology because of the gas involved in the reaction so it is still in the experimental research stage. Compared with sensible heat storage materials, these two kinds of heat storage materials have a limited application range. Therefore, sensible materials are more suitable for high-temperature thermal energy storage systems, have higher practical application values, and are the most commonly used materials for storing solar energy at present.[11,12]

At present, the most commonly used thermal energy storage system for concentrating solar power plants is based on the concept of two-tank storage that using molten salt as the heat storage medium, and solar salt Hitec and Hitec XL (a mixture of nitrate and nitrite) are usually used. However, molten salts are unstable at high temperatures, such as nitrates, nitrites, and carbonates decomposing at temperatures higher than 600 °C, which limits their application in the high-temperature field.[13] Furthermore, the solidification point of molten salts is relatively high (100−200 °C)[14] so the working temperature range is small, and thus, the heat storage density that is positively correlated with the operating temperature range is significantly weakened. In fact, the operating temperature of the tower concentrating system is as high as 1500 °C, and the energy above 600 °C is still not well stored and utilized. Moreover, molten salts are corrosive to pipes and equipment[15] and can greatly increase investment costs. Compared with the existing thermal storage technology, the packed bed mode, in which the solid material is the heat storage medium and the air is the heat transfer fluid, is considered to be an excellent alternative to improve the efficiency and economic benefit of the storage system.[16]

Some scholars have studied the heat storage potential of natural rocks. Due to the uncertain natural formation process, the chemical composition of natural rocks from different geological locations varies greatly. Some inclusions and impurities will cause chemical inhomogeneities in the rock. Some components in the rocks such as water and silanol can be volatilized or decomposed at high temperature[17]and can lead to cracks inside the materials, which greatly weaken their mechanical properties and thermophysical properties.[18] Some studies have found that preheat treatment of rocks can effectively avoid cracking during continuous heating−cooling cycles.[19] Hanley et al.[20] found that the thermal diffusivity of the rock heated to 727 °C and cooled to 27 °C would exceed 30−40% of that of untreated rock. Grirate et al.[21] studied the heat storage potential of six rocks (quartzite, basalt, granite, hornfels, cipolin, and marble) in Morocco and found that basalt has higher heat capacity than other rocks and shows the best thermal performance in the concept of thermocline storage systems. Basalt is the raw material for preparing basalt fibers, and the fibers have excellent properties such as high tensile strength, high-temperature resistance, erosion resistance, thermal insulation, etc.[22] They are widely used as basic materials for various composite materials. Basalt glass is an intermediate product for preparing basalt fiber.[23] Melting and quenching natural basalt and annealing at a certain temperature can produce a uniform and stable glass system. In the melting process, impurity components can be removed, thermal expansion performance can be improved, and the density of the system can be increased, thus obtaining ideal mechanical properties and thermophysical properties. Basalt glass is an amorphous material with no lattice defects. It is in a viscous fluid state at high temperature, but it does not flow. It has good processability and can freely adjust its shape and size. Therefore, basalt glass can also be used in mobile heat storage systems to realize long-distance heat transfer. In this paper, the effects of temperature and composition on the thermophysical properties of basalt glass are studied, and its feasibility as a heat storage material is specifically analyzed.

2. RESULTS AND DISCUSSION

2.1. Composition and Structural Analysis. The chemical composition of the basalt glasses was analyzed using an X-ray fluorescence spectrometer (XRF), and the molar percentages of the basic component of the glasses are presented in Table 1. It can be noticed that silica is the predominant component of the three samples, which acts as the glass network former, and the basic network skeleton of the glass system is formed in the $[SiO_4]$ tetrahedron. Compared with ordinary glasses and ores, basalts contain more iron oxide (4−7 mol %), which will have a great impact on the thermophysical properties such as crystallization temperature and viscosity.[24,25] Among the studied samples, the content of alumina in the network intermediate showed a weak variation. Alumina can combine with the free oxygen in the glass to participate in the network formation with the four-coordinate $[AlO_4]$, which plays the role of network compensation. It will also enter the gap of the glass network in the form of six-coordinate $[AlO_6]$. In addition, a small amount of alkali metal oxides and alkaline earth metal oxides are included, and weak changes in these components also have a significant effect on the structure and properties of the sample.

The state of the glass network intermediate Al_2O_3 in the glass system is determined by the amount of free oxygen provided by the alkali metal and alkaline earth metal oxide, and 1 mole of free oxygen can be used for 1 mole of Al_2O_3 to form $[AlO_4]$. The amount of free oxygen can be calculated by eq 1

$$N_{\text{free oxygen}} = \sum K_i \times M_i \quad (1)$$

https://dx.doi.org/10.1021/acsomega.0c02773
ACS Omega 2020, 5, 19236−19246

$N_{free\ oxygen}$ represents the amount of free oxygen, K_i is the oxygen supply coefficient of the oxide, as listed in Table 2, and

Table 2. Oxygen Supply Coefficient of Various Oxides

oxide	CaO	MgO	K_2O	Na_2O
K_i	0.4	0.2	1	1

M_i represents the mole fraction of the oxide.[26] According to eq 1, the free oxygen contents of the three glass systems BG-1, BG-2, and BG-3 were 10.32, 9.93, and 13.07 mol %, respectively. Except that the amount of free oxygen of BG-1 is slightly smaller than that of Al_2O_3 (10.72 mol %), the others are higher than the Al_2O_3 content of the respective systems. Therefore, Al_2O_3 in all three glasses can be considered to be composed of $[AlO_4]$ tetrahedrons participating in the network, and it functions as the network former. Depending on the basic structure theory of silicate glass melt,[27] $[SiO_4]$ and $[AlO_4]$ tetrahedrons form a complex three-dimensional network structure by sharing oxygen ions and connecting corners and tops.[28] The higher their content, the higher the polymerization degree of glass.[22,29] Therefore, according to the composition of the three kinds of basalt glass, it can be preliminarily inferred that the structural stability of the three kinds of basalt glass decreases in turn, which is verified by subsequent tests.

The infrared spectra of basalt ores and glasses are shown in Figure 1, wherein the wavenumber ranges from 500 to 4000

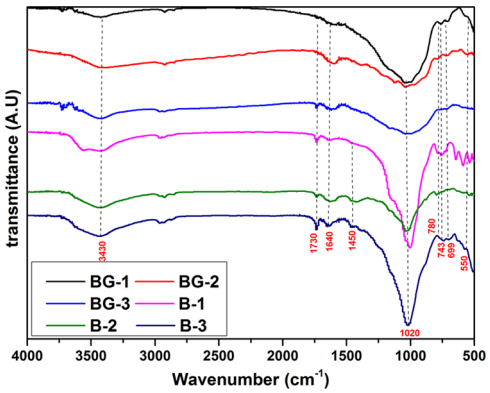

Figure 1. IR spectra of basalts and basalt glasses at room temperature.

cm^{-1}. The small shoulder located at 550 cm^{-1} can be attributed to the Si−O−Al bending vibration of $[SiO_4]$ and $[AlO_4]$ tetrahedral structural units.[30,31] The band observed at around 699 cm^{-1} is due to the Al−O stretching vibration of the $[AlO_4]$ tetrahedron.[31,32] The Fourier transform infrared (FTIR) spectra exhibit weak peaks at 743 and 780 cm^{-1}, which can be assigned to the Si−O−Si symmetric stretching vibration and the Si−Si stretching vibration.[32] The broadband observed between 850 and 1250 cm^{-1} is related to the asymmetric stretching vibration of Si−O−Si, Si−O−Al, and Si−O bonds.[30] The peak near 1020 cm^{-1} is attributed to the $[SiO_4]$ tetrahedron and a nonbridged oxygen atom vibration.[33] It can be concluded that the network skeletons of basalt ores and glasses are mainly composed of the $[SiO_4]$ tetrahedron and the $[AlO_4]$ tetrahedron, which also confirms the reliability of the calculation of the structure type. Weak peaks that appear at 1450, 1640, and 1730 cm^{-1} are assigned to the H−O−H bending vibration of adsorbing water.[34,35] Obviously, these peaks of basalt glasses are weakened or even disappeared, indicating that the content of adsorbed water is significantly reduced after the basalt ores are melted. The peak near 3430 cm^{-1} is attributed to the presence of silanol hydroxyl groups: Si−OH deformation and stretching vibration,[35,36] where the peaks of basalt glasses have significantly weakened, indicating the decrease of the Si−OH content.

2.2. Thermophysical Characterization. *2.2.1. Thermal Stability.* Solid heat storage materials must not be able to melt in the working temperature range. Thermal stability analysis is critical to assessing thermal storage performance, so as to predict the appropriate working temperature of the thermal storage materials and the possible physical and chemical reactions during the thermal cycle. In this work, thermogravimetry (TG)−differential scanning calorimetry (DSC) analysis of basalts and glasses was carried out in the temperature range of 40−1200 °C and three heating/cooling cycles were performed at a temperature change rate of 20 °C/min to evaluate the thermal cycling resistance. Figure 2a−c displays the TG curves of three heating−cooling cycles of basalts. It can be observed that the three samples have obvious mass loss during the first heating process and the mass loss rate is about 1.91, 5.18, and 2.04%, respectively, with sample B-2 having the largest mass loss.

Figure 3a shows the DSC analysis curves of basalts, wherein the heating rate is 20 °C/min. Combined with TG−DSC analysis, the three samples undergo the same reaction when they are heated for the first time. Below 200 °C, the mass loss is attributed to the escape of the adsorbed water, and sample B-2 has a higher adsorbed water content of about 1.7%. In 200−800 °C, due to the decomposition reaction of silanol, new Si−O−Si bonds and water molecules are produced.[37] Water molecules are encapsulated in the closed pores of the network skeleton, the vapor pressure increases with increasing temperature, and the stress causes the internal atomic bonds to break, which then leads to the occurrence of cracks.[18] The ores can be regarded as polycrystals composed of various mineral phases. There is an endothermic peak on each DSC curve at around 580 °C, which is the transformation of the quartz phase from α to β.[17] Owing to the higher content of quartz in B-1, the peak shape is sharper, and the peak shapes of B-2 and B-3 are gradually broadened. However, due to the large thermal expansion coefficient of β-quartz, the rock will crack during the heating process, thus limiting its working temperature.[38] The escape of water molecules due to silanol decomposition and the phase transition of quartz will give rise to material fracture. To maintain the high heat storage performance and long service life, the ideal maximum working temperature of these basalts are only 500 °C. It is worth noting that sample B-2 has an additional endothermic peak on the DSC curve between 700 and 800 °C. This may be the conversion of the olivine phase to hematite (Fe_2O_3).[39] Because of the high Fe content in B-2, this peak is more evident.

In contrast, the three glass samples showed almost no mass loss during the three cycles, as shown in Figure 2d for the TG curve of BG-1 (the other two glasses have the same trend, and here were not presented to avoid the picture redundant). The TG curve fluctuates, and there is an upward trend at around 660 °C. This may be due to the thermal effect of the glass transition, resulting in uneven temperature distribution around the sample, producing gas convection and heavy gas sinking, and causing apparent weight gain. TG curves show that the volatile and decomposable impurities are removed, and the

https://dx.doi.org/10.1021/acsomega.0c02773
ACS Omega 2020, 5, 19236−19246

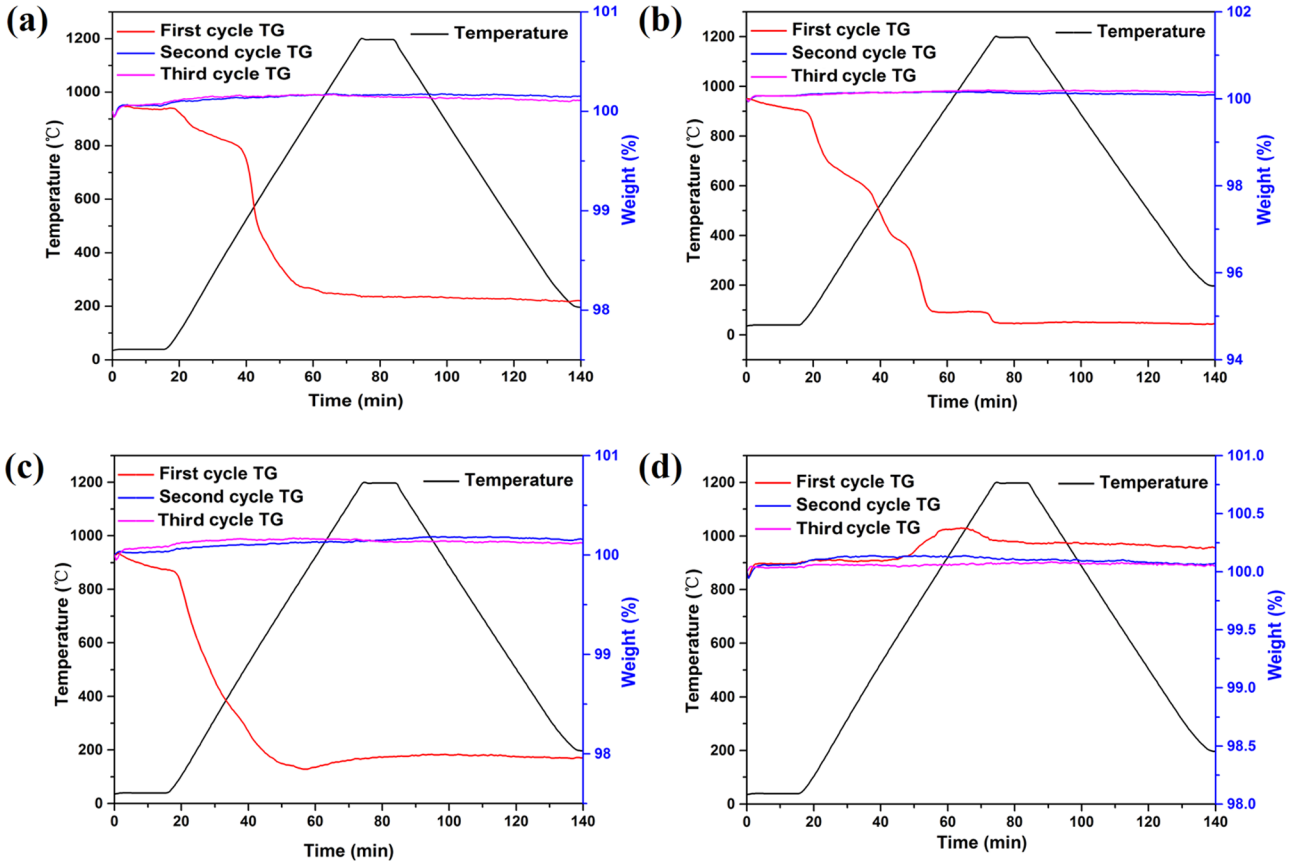

Figure 2. TG curves of basalts and basalt glass: (a) B-1, (b) B-2, (c) B-3, and (d) BG-1.

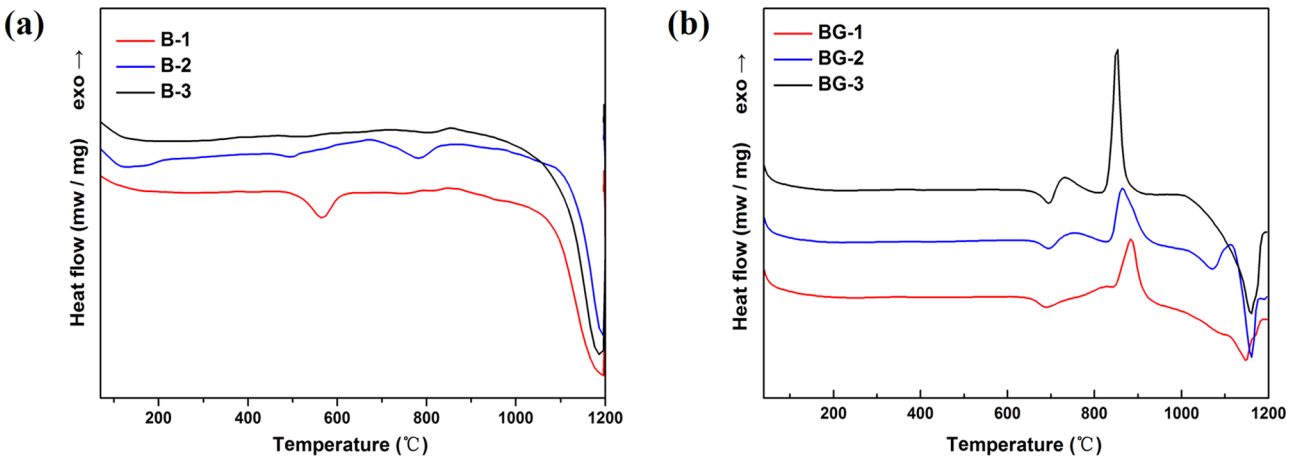

Figure 3. DSC analysis: (a) basalt ores and (b) basalt glasses.

thermal stability is greatly improved after the basalt ores are melted into glasses.

As shown in Figure 3b, the three glasses have both endothermic and exothermic peaks on the DSC curve (the heating rate is 20 °C/min), and the first endothermic peak represents the glass transition point. The glass transition temperature T_g of the three samples is not much different, varied between 663 and 669 °C. The first exothermic peak corresponds to the crystallization temperature T_p. The temperature of the crystallization peak can be observed to decrease sequentially, which are 884, 864, and 851 °C, respectively, and the peak gradually becomes sharp. As the content of the network former decreases, the glass network becomes loose, the glass melt is more likely to suffer phase separation, more nucleation sites are provided, and crystal nucleus are easy to form and grow. Moreover, BG-2 and BG-3 contain more Fe_2O_3 and TiO_2. Since the bond energy of Fe−O (397.48 kJ/mol) is smaller than that of Al−O (481.16 kJ/mol) and Si−O (774.04 kJ/mol),[25] the $[FeO_4]$ tetrahedron is unstable in glass. During the heat treatment, part of the Fe−O bond is broken, resulting in the decrease of viscosity, thereby increasing the nucleation efficiency. It also leads more crystal nuclei to be formed in the glass and reduces the temperature of the crystallization peak. Moreover, TiO_2 can promote phase separation and reduce interfacial energy and crystallization activation energy.[40] The last endothermic peak in the DSC

https://dx.doi.org/10.1021/acsomega.0c02773
ACS Omega 2020, 5, 19236−19246

curve stands for the melting peak of the glass, and the melting peak temperature T_m of all of the glasses is higher than 1100 °C.

The above description confirms that the analyzed basalt glasses have excellent thermal shock resistance compared to basalts. The BG-1 sample has more SiO_2 and Al_2O_3 as network formers, and a small amount of oxides that promote nucleation. The glass network structure is more compact, which is beneficial to the conduction of heat, reduces the thermal stress during the charge and discharge of the glass system, and avoids the generation of cracks. Since the melting temperatures of the three glasses are higher than 1100 °C, it is preliminarily concluded that the maximum working temperature of the basalt glasses used as sensible heat storage materials can reach 1000 °C. It can also be found from Figure 5 that the glasses do not melt when heated to 1000 °C.

2.2.2. Thermal Expansion. Thermal expansion performance is a prominent factor in determining the thermal stability of a thermal storage material. The heat storage material requires the thermal expansion coefficient to be as small as possible to reduce the volumetric stress caused by temperature change during the thermal cycle to prolong its service life and improve its safety. When the temperature rises, the vibration amplitude of the particles in the glass increases, and the distance between the particles increases accordingly so the glass expands. Thermal expansion is negative to the bond strength of the glass component and the tightness of the network. The thermal expansion curves of the three glass samples between 40 and 750 °C are presented in Figure 4, and the heating rate is 5 °C/min. The obtained result illustrates that the variation of the length of samples increases linearly with a temperature between 40 and 650 °C, and a steep increase in the slope of the thermal expansion curves when the temperature is higher than 650 °C. This is due to the glass transition that occurred at around 650 °C, the glass network becoming loose, and the characteristic of the melt state that begins to occur.

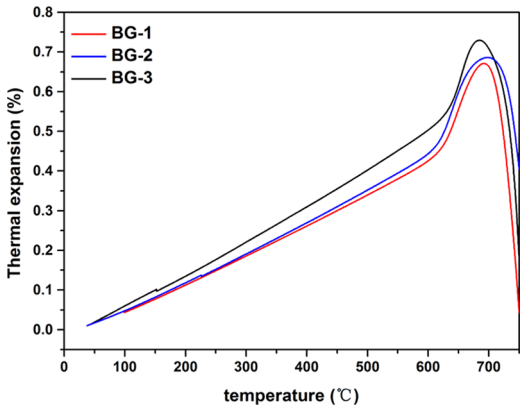

Figure 4. Evolution of the thermal expansion of basalt glasses.

The highest point of the thermal expansion curve indicates the softening point of the glass, and the softening temperatures are 686.5, 697, and 684.6 °C, respectively, and the maximum length variable is between 0.6 and 0.7%. After the softening point temperature, the movement ability of atoms is enhanced, the pores of the network structure will be filled rapidly, and the microcracks will be healed to compensate for the thermal expansion effect, resulting in negative thermal expansion. This shows that basalt glasses are more favorable for high-temperature use. Ding et al.[41] conducted a molecular dynamics simulation study on the thermal expansion properties of quartz glass, confirming the negative expansion phenomenon.

Figure 5 displays the contour picture of basalt glasses at a high temperature, showing that the volume hardly changes with increasing temperature without being subjected to an external force. The linear thermal expansion coefficients of the three samples vary between 7.63 and 8.91 × 10^{-6} °C^{-1}, which are significantly lower than that of flint (16−18 × 10^{-6} °C^{-1}),[37] Egypt and France basalts (10 × 10^{-6} °C^{-1}),[39] high-temperature concrete (9.3 × 10^{-6} °C^{-1}), and castable ceramic (11.8 × 10^{-6} °C^{-1}),[42] indicating that basalt glasses possess good thermal shock resistance and are suitable candidates for heat storage materials. The thermal expansion coefficients of the studied basalt glasses are slightly different, and the value of BG-1 is relatively low, which also confirms that the network structure of BG-1 is more stable.

2.2.3. Density. The measured density values of the studied samples at room temperature are exhibited in Table 3 with density values of other materials obtained from the literature. It can be observed that BG-2 and BG-3 have almost the same density, while the density value of BG-1 is slightly smaller. In fact, the first two samples have more network modified oxides, and the alkali metal ions and alkaline earth metal ions are filled into the [SiO_4] and [AlO_4] tetrahedral network interspace to make the system denser so the density values are slightly larger. We assume that the density of basalt glass remains constant at high temperatures because of its small coefficient of thermal expansion. This can also be demonstrated by contour images at different temperatures, as shown in Figure 5. After the studied glasses were heated from room temperature to 1000 °C and kept for 2 h, the volume of the glasses did not change significantly. Compared to the reported sensible heat storage materials, such as solar salt Hitec (1.899 g/cm^3)[43] and high strength concrete (2.250 g/cm^3),[44] the analyzed basalt glasses show higher density. According to eq 2, they have obvious advantages in heat storage.

2.2.4. Specific Heat Capacity and Thermal Capacity. The volumetric heat capacity ($\rho \times C_p$) is a physical property that characterizes the amount of thermal energy stored in a heat storage material. It is the most important parameter in thermal storage applications and has a significant impact on the thermal efficiency and investment of the thermal storage system.[45,46] Furthermore, the widely recognized volumetric heat capacity must be higher than 1000 KJ/(m^3·K).[47] The heat storage density represents the total heat energy stored in a unit volume of heat storage material during one thermal cycle. According to eq 2, the heat storage density is positively correlated with the volumetric heat capacity and the working temperature range. As this property increases, it can reduce the storage volume required for thermal storage systems, improve economic efficiency, and be more competitive in commercial applications.

In Figure 6a−c, the experimentally measured specific heat capacity C_p of basalt glasses was plotted in the temperature range of 40−1000 °C during three thermal cycles, and the solid line indicates the heating process. During the first heating process, the peaks appeared on the specific heat curve, which is due to an exothermic or endothermic reaction at the peak temperature, which corresponds to the glass transition and crystallization processes, respectively. This will affect the measurement of the actual specific heat capacity, and the true specific heat value around the endothermic and

https://dx.doi.org/10.1021/acsomega.0c02773
ACS Omega 2020, 5, 19236−19246

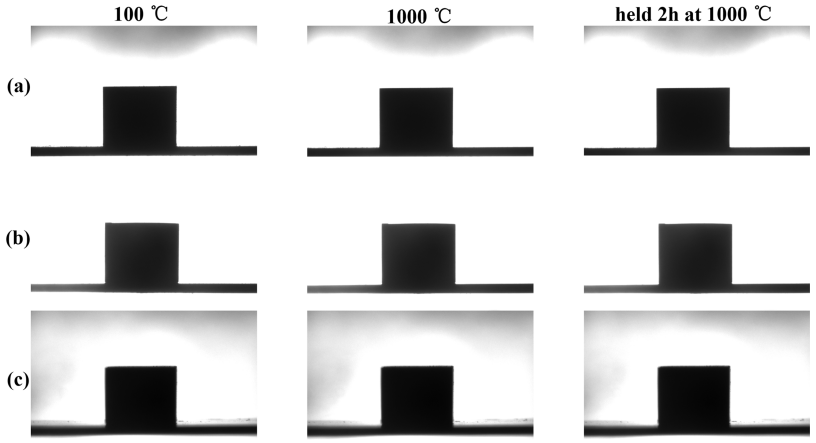

Figure 5. Contour pictures of basalt glasses at different temperatures: (a) BG-1, (b) BG-2, and (c) BG-3.

Table 3. Density of Basalt Glasses and Other Storage Materials Given in Literature at Room Temperature

sample	BG-1	BG-2	BG-3	solar salt	concrete
density (g/cm^3)	2.66	2.85	2.81	1.899	2.25

exothermic areas can be obtained by interpolation. Nevertheless, in the subsequent two heating processes, BG-1 and BG-3 had no obvious endothermic and exothermic peaks. This implicates that the first thermal cycle has allowed the glass system to relax for a sufficient time, and the internal energy is released to reach a more stable equilibrium state. It is worth mentioning that BG-2 still has crystallization peaks in the subsequent two heating processes, which may be due to the high Fe_2O_3 content that makes it difficult to reach the energy equilibrium state and easy to devitrify. It can be observed that during the three consecutive heating and cooling processes, the specific heat value of each sample at the same temperature

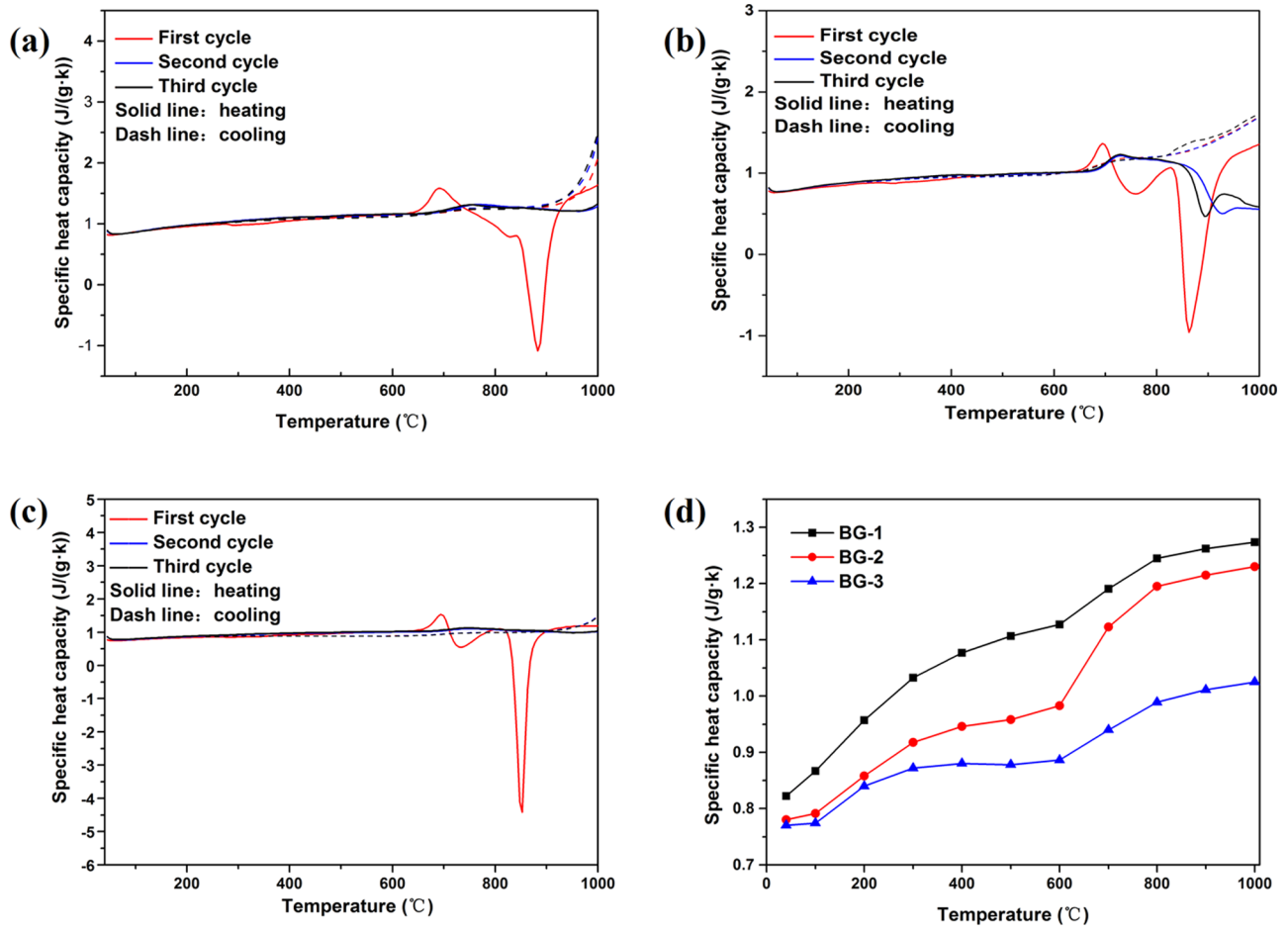

Figure 6. Specific heat capacity vs temperature of basalt glasses. Experimental measurements: (a) BG-1, (b) BG-2, (c) BG-3 and fitted values, and (d) three glass samples.

https://dx.doi.org/10.1021/acsomega.0c02773
ACS Omega 2020, 5, 19236−19246

hardly changes because of the fixed composition, which proves that the studied basalt glasses possess good thermal cycling stability.

The specific heat capacity of basalt glasses at different temperatures are presented in Table 4, and the real change in specific heat capacity as a function of temperature is fitted in Figure 6d. Obviously, the specific heat capacity of the three glass samples varies similarly with temperature, and the specific heat value generally increases with temperature. This is due to the fact that the specific heat of solids is the sum of the contributions of atomic vibrations at various frequencies. As the temperature increases, the degree of freedom of atomic vibrations increases so the specific heat increases.[48] In addition, the specific heat capacity rapidly rises below 300 °C, the atomic vibrations are frozen at very low temperatures and trapped in the energy potential well, and the number of "thawed" atoms increases rapidly with increasing temperature. The increase of specific heat capacity between 300 and 600 °C becomes slow and gradually reaches a constant value, which is in line with the Dulong and Petit law. The specific heat abruptly changes between 600 and 800 °C, this is due to the rapid decrease in glass viscosity after the glass transition temperature and the transition from a dense structure to a loose structure. It has meltlike properties and increases the freedom of atomic vibration; the sudden increase in specific heat capacity is called configurational entropy, and then, the specific heat stabilizes.

Table 4. Specific Heat Capacity of Basalt Glasses at Different Temperatures (J/(g·k))

temperature (°C)	40	200	400	600	800	1000
BG-1	0.822	0.957	1.077	1.127	1.245	1.274
BG-2	0.780	0.858	0.946	0.983	1.195	1.230
BG-3	0.770	0.840	0.880	0.886	0.989	1.025

In detail, the specific heat capacities slightly vary from 0.822 to 0.770 J/(g·K) at 40 °C for BG-1, BG-2, and BG-3, and the C_p values that rise to reach maximum values vary from 1.274 to 1.025 J/(g·K) at 1000 °C, which increased about 55, 58, and 33%, respectively. The average specific heat capacity of the ceramics that are certified as sensible heat storage materials is 0.85 J/(g·K) in the range of 200−400 °C,[43] and the C_p values of basalt glasses analyzed in this study are significantly higher than this value. The average specific heat capacity of solar salt Hitec at the working temperature between 220 and 600 °C is 1.5 J/(g·K).[43] Although the specific heat capacities of basalt glasses are lower than this value, the density is remarkably higher than that of solar salt so they have higher heat capacity values. The thermal capacity of each basalt glass is calculated by multiplying its specific heat capacity and density, and the obtained results are presented in Figure 7. It can be observed that before 700 °C, BG-1 has the largest thermal capacity. At higher temperatures, the thermal capacity of BG-2 even exceeds BG-1 due to its higher density. The average volumetric thermal capacities of basalt glasses between 100 and 1000 °C are 3.164, 2.915, and 2.28 MJ/(k·m^3), and the heat storage densities calculated by eq 2 in this temperature range are 2847.6, 2623.5, and 2052 MJ/m^3, respectively. The thermal capacity of currently preferred molten nitrates is 3.0 MJ/(k·m^3),[43] limited to the working temperature range of about 300 °C so it can store only 900 MJ/m^3 of heat, which shows that basalt glasses have enormous advantages in terms of heat storage.

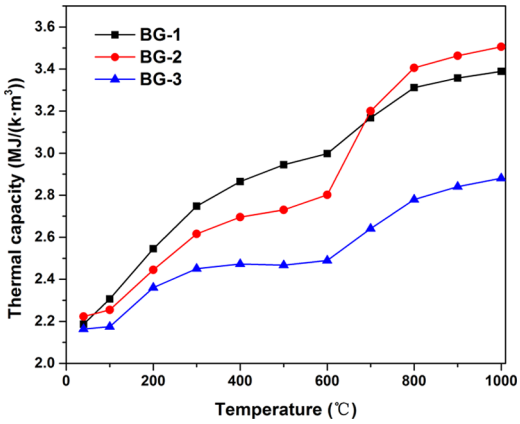

Figure 7. Thermal capacity of the studied basalt glasses.

2.2.5. Thermal Diffusivity and Thermal Conductivity. Thermal diffusivity and thermal conductivity determine the efficiency of charge and discharge in heat storage materials.[49] The materials need to have sufficiently high thermal conductivity that should be greater than 1 W/(m·K),[50] to allow the heat to quickly transfer between inside and the surface so that each part of the materials has a smaller temperature gradient[51] so as to reduce the thermal stress of the heat storage material and improve the heat exchange performance of the TES. Measuring the thermal diffusion coefficient is an indirect method for obtaining thermal conductivity. The measured value of the thermal diffusion coefficient as a function of temperature is shown in Figure 8a, and the error bars in the figure representation correspond to the standard deviations of three measurements at the same temperature. In Figure 8a, the similarity of the thermal diffusivity curves of basalt glasses is evident. Between 200 and 750 °C, the thermal diffusion coefficient decreases slightly with increasing temperature. This is because the heat conduction of solid materials depends on the motion of phonons, and as the temperature increases, the number of phonon collisions increases and hence the average free path of phonons decreases. Within this temperature range, the thermal diffusion coefficient of the studied samples decreases from 0.46 to 0.41 mm^2/s (about 11%), 0.44 to 0.41 mm^2/s (about 7%), and 0.43 to 0.38 mm^2/s (about 12%), respectively. The thermal diffusion coefficient increases slightly above 750 °C, which may be due to the filling of structural pores and microcracks leading to an increase in heat transfer of basalt glasses. It is worth noting that the thermal diffusion coefficient of BG-1 is higher than those of BG-2 and BG-3, which is attributed to the high content of SiO_2 in BG-1, and quartz has the highest thermal diffusion coefficient among the major minerals (3.8 mm^2/s).[52] Hanley et al.[20] demonstrated that rocks with a high content of silica (SiO_2), such as Berea sandstone or quartzite, tend to have high thermal diffusivity, while limestone and marble have low thermal diffusion coefficients because they do not contain quartz.

As shown in Figure 8b, the thermal conductivity of the studied glasses was calculated from eq 3 increases as a function of temperature, which is consistent with the change in the thermal conductivity of most glasses. The thermal conductivities of basalt glasses at 200 °C are 1.19, 1.07, and 1.02 W/(m·K), respectively. BG-1 has the highest thermal conductivity,

https://dx.doi.org/10.1021/acsomega.0c02773
ACS Omega 2020, 5, 19236−19246

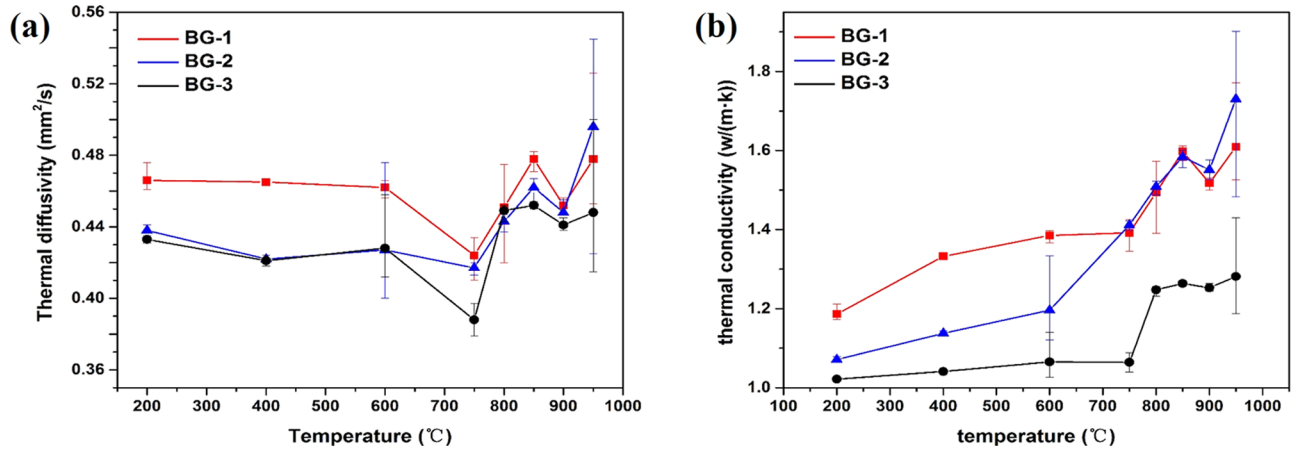

Figure 8. (a) Thermal diffusion coefficient and (b) thermal conductivity as a function of temperature for different basalt glasses.

Table 5. Chemical Compositions of Raw Basalt Stones (wt %)

(wt %)	SiO_2	Al_2O_3	Fe_2O_3	CaO	MgO	SO_3	TiO_2	K_2O	Na_2O	P_2O_5	others
B-1	53.66	15.49	8.97	6.59	4.84	0.03	0.88	2.17	3.36	0.39	3.62
B-2	48.07	13.52	16.04	9.39	4.26	0.04	3.06	0.98	2.68	0.00	1.96
B-3	43.42	14.00	12.82	9.13	8.96	0.03	2.99	1.69	3.47	0.72	2.77

and BG-3 has the lowest one because SiO_2 with high thermal conductivity can significantly improve the thermal conductivity of glass. In addition, most of $[SiO_4]$ and $[AlO_4]$ in BG-1 are connected by a framework structure, and the structure has a high degree of polymerization and order, which is conducive to phonon transmission. Before 700 °C, the change in thermal conductivity of the three samples is relatively gentle. The thermal conductivity increases rapidly after the softening point temperature, and BG-2 has the fastest growth and even reaching the level of BG-1. It is worth mentioning that the basalt glasses analyzed in this study exhibit higher thermal conductivity compared to solar salts (0.52 W/(m·K)) and thermal oil (0.1 W/(m·K)).[43] Therefore, the basalt glasses show obvious advantages in terms of thermal conductivity, which will help to improve the performance and efficiency of the thermal energy storage system.

3. CONCLUSIONS

In this work, the thermophysical properties of different types of basalt glasses have been successfully measured and compared with basalt ores in terms of structure and thermal stability. The obtained results demonstrate that basalt glasses have better heat storage performance than ores. After the high-temperature melting process, the volatilizable and decomposable impurities such as water and silanol are removed and the thermal stability is improved. Furthermore, the working temperature range is greatly improved up to 1000 °C, while the maximum working temperature of these basalts is only 500 °C. It is worth mentioning that the studied basalt glasses have very low coefficients of thermal expansion. They will self-heal pores and microcracks at high temperatures, resulting in negative thermal expansion and a rapid increase in thermal conductivity. Remarkably, there is almost no variation in volume when heated to 1000 °C. Moreover, it has been concluded that these basalt glasses are suitable candidates for concentrated solar power plants and home heating systems.

In detail, among the three basalt glass studied in this work, BG-1 prepared from intermediate basalt has better comprehensive thermophysical properties. In fact, larger amounts of SiO_2 promotes the formation of a $[SiO_4]$ polymerized network, and the lower O/(Si + Al) molar ratio also improves the structural stability, thereby reducing the coefficient of thermal expansion. In addition, the obtained results showed that BG-1 also has higher specific heat capacity, heat capacity, and thermal conductivity. The mean value of heat capacity between 100 and 1000 °C is 3.164 MJ/(k·m^3), and each cubic meter of BG-1 can store 2847.6 MJ of heat in this temperature range. The thermal conductivity during thermal cycling from 200 to 1000 °C is 1.19−1.60 W/(m·K). In summary, compared with other sensible heat storage materials, basalt glasses studied in this work not only have the characteristics of low cost and being environmentally friendly but also have higher heat capacity, thermal conductivity, and excellent thermal stability between 100 and 1000 °C. Finally, the research content included in this work has a reference value for the effective use of other natural ores, and the effect of the composition on the thermophysical properties of ores and glasses has been analyzed in detail, so as to better predict and optimize the thermal storage performance of such materials.

4. MATERIALS AND METHODS

4.1. Sample Selection and Preparation. In mineralogy, natural basalts can be divided into intermediate basalt (SiO_2 content is between 53 and 66 wt %), basic basalt (SiO_2 content is between 45 and 53 wt %), and ultrabasic basalt (SiO_2 content is less than 45 wt %). There are large differences in the structure and properties of different types of basalt. Three typical samples from these three kinds of basalts were picked and recorded as B-1, B-2, and B-3, respectively. The composition of the basalts is shown in Table 5. A total of 1000*g* of each basalt was weighed and was crushed; the powder was transferred to a platinum crucible and dried at 200 °C for 1 h, subsequently kept at 1500 °C to enable it to clarify and homogenize. After 3 h, part of the melt was quenched in water and then milled into 200-mesh powder for DSC testing and component analysis. The rest was transferred to a preheated

https://dx.doi.org/10.1021/acsomega.0c02773
ACS Omega 2020, 5, 19236−19246

550 °C steel plate. After annealing at 500 °C for 2 h in a muffle furnace and cooling with the furnace, basalt glasses can be obtained, which were respectively recorded as BG-1, BG-2, and BG-3.

4.2. X-ray Fluorescence (XRF). The composition of basalt glasses was analyzed using an X-ray fluorescence spectrometer 9900 X-ray workstation produced by the American Thermo Fisher. A total of 1 g of basalt glass powder for analysis was placed in a crucible containing 5 g of 100% pure $Li_2B_4O_7$, and then 3 drops of LiBr saturated solution was added to it. It was then transferred to a fully automatic multi-head melting machine, and its chemical composition was determined after the glass frit was cooled.

4.3. Fourier Transform Infrared (FTIR) Spectra. To determine the structural and chemical stability of the studied rocks and glass, Fourier transform infrared analysis was carried out using a Thermo Fisher Nicolet iS10 spectrometer. Pellets made of a mixture of powdered glass and KBr in a weight ratio of 1:50, respectively, which have been placed in a mold and pressed into sheets for measurement. The absorption spectra were recorded in the range 400−4000 cm^{-1} and obtained with an accumulation of 16 scans.

4.4. Differential Scanning Calorimetry (DSC). The specific heat capacity C_p is an important index of the sensible heat storage material. The heat capacity is the product of density (ρ) and C_p. The heat storage density is calculated by multiplying the mean values of heat capacity and the applicable temperature interval, which can be expressed by eq 2

$$M = \rho \times C_p \times \Delta T \tag{2}$$

where M represents the volumetric heat storage density (J/m^3) and ΔT is the applicable temperature range of the material. It can be seen that the larger the C_p value is, the more heat energy is stored per unit volume of material. The glass transition temperature T_g, crystallization temperature T_p, and specific heat capacity C_p of the samples were measured by DSC using a Netzsch STA 449 F3 differential scanning calorimeter. The instrument can simultaneously measure the TG−DSC curve, the purge gas and protective gas are in an argon atmosphere, the gas flow rates are 60 and 20 mL/min, respectively, and the sample to be tested is in the platinum crucible. To improve the detection sensitivity of the weak thermal effect to obtain the accurate value of specific heat capacity, 60 mg of powder samples is added to platinum crucibles with lids and the heating/cooling rate is set to 20 °C/min.[53] When the specific heat of the sample is measured, the baseline test is performed on the empty crucible within the temperature range, then the sapphire standard sample is tested, and finally the sample is run and the specific heat value is determined by the ASTME 1269 standard thermal analysis method.

4.5. Thermal Expansion. The thermal expansion coefficient was measured using the German Netzsch TMA 402F1. Cuboid samples (4 × 5 × 25 mm) were prepared and polished to ensure parallel ends. The standard alumina sample was heated at 5 °C/min to 750 °C to make a thermal expansion baseline, and then the tested sample was measured according to the same temperature procedure.

4.6. Density. The density of the sample was determined by the Archimedes method at room temperature, each sample was measured five times, and then the average value of the measured values was taken as the actual density.

4.7. High-Temperature Contour. The prepared basalt glasses were processed into a 4 × 5 × 5 mm square block, and a high-resolution camera equipped with the Dataphysics OCA 20LHT high-temperature contact angle measuring instrument was used to record the contour change of the glass block at different temperatures.

4.8. Laser Flash. In this work, the thermal diffusivity of basalt glasses was measured by the laser flashing method using a Netzsch LFA 427 instrument. The basalt glasses were made into a square sample (10 × 10 × 1.5 mm), and the measurement was carried out under an argon atmosphere at a heating rate of 2.5 °C/min. Three valid data were collected at each temperature point between 200 and 1000 °C, and each presented experimental result represents the average of three measured values at the same temperature. The thermal conductivity (λ) of the prepared glasses was calculated by multiplying thermal capacity ($\rho \times C_p$) and thermal diffusivity (α), which can be expressed by eq 3

$$\lambda(T) = \rho \times C_p(T) \times \alpha(T) \tag{3}$$

AUTHOR INFORMATION

Corresponding Authors

Jianxun Liu − *School of Civil Engineering and National & Local Joint Engineering Research Center of "Basalt Fiber Production and Application", Southeast University, Nanjing 210096, China*; orcid.org/0000-0002-6660-6879; Phone: +86 13382095760; Email: jxliu@seu.edu.cn

Rao Kuang − *School of Energy and Environment and Key Laboratory of Solar Energy Science and Technology in Jiangsu Province, Southeast University, Nanjing 210096, China*; Phone: +86 13951665754; Email: 101011329@seu.edu.cn

Zhishen Wu − *School of Civil Engineering and National & Local Joint Engineering Research Center of "Basalt Fiber Production and Application", Southeast University, Nanjing 210096, China*; Email: zswu@seu.edu.cn

Authors

Zhongchen Chang − *School of Materials Science and Engineering and National & Local Joint Engineering Research Center of "Basalt Fiber Production and Application", Southeast University, Nanjing 210096, China*

Lianbo Wang − *School of Materials Science and Engineering and National & Local Joint Engineering Research Center of "Basalt Fiber Production and Application", Southeast University, Nanjing 210096, China*

Jingwen Xu − *School of Energy and Environment and Key Laboratory of Solar Energy Science and Technology in Jiangsu Province, Southeast University, Nanjing 210096, China*

Complete contact information is available at: https://pubs.acs.org/10.1021/acsomega.0c02773

Notes

The authors declare no competing financial interest.

ACKNOWLEDGMENTS

This work was financially supported by the National Key R&D Program of China [2017YFB 0310904] and the Fundamental Research Funds for the Central Universities [2242018K41044].

https://dx.doi.org/10.1021/acsomega.0c02773
ACS Omega 2020, 5, 19236−19246

ABBREVIATIONS

XRF	X-ray fluorescence
FTIR	Fourier transform infrared
DSC	differential scanning calorimeter
TMA	thermomechanical analyzer
LFA	laser flash analyzer
TES	thermal energy storage
PCMs	phase change materials

NOMENCLATURE

ρ	density (g/cm^3)
C_p	specific heat capacity (J/(g·K))
α	thermal diffusivity (mm^2/s)
λ	thermal conductivity (W/(m·K))
T	temperature (°C)
M	volumetric heat storage density (J/m^3)
$N_{\text{free oxygen}}$	the amount of free oxygen
K_i	oxygen supply coefficient
M_i	mole fraction of the oxide

REFERENCES

(1) Iten, M.; Liu, S.; Shukla, A. A Review on the Air-PCM-TES Application for Free Cooling and Heating in the Buildings. *Renewable Sustainable Energy Rev.* **2016**, *61*, 175−186.

(2) Hasnain, S. M. Review on Sustainable Thermal Energy Storage Technologies, Part I: Heat Storage Materials and Techniques. *Energy Convers. Manag.* **1998**, *39*, 1127−1138.

(3) Kuravi, S.; Trahan, J.; Goswami, D. Y.; Rahman, M. M.; Stefanakos, E. K. Thermal Energy Storage Technologies and Systems for Concentrating Solar Power Plants. *Prog. Energy Combust. Sci.* **2013**, *39*, 285−319.

(4) Tian, Y.; Zhao, C. Y. A Review of Solar Collectors and Thermal Energy Storage in Solar Thermal Applications. *Appl. Energy* **2013**, *104*, 538−553.

(5) Samala, S.; Brahma, G. S.; Swain, T. Synthesis and Characterization of Sensible Thermal Heat Storage Mixture Containing Phosphate Compound of Cobalt and Sodium. *Sol. Energy* **2019**, *177*, 612−619.

(6) Konuklu, Y.; Ostry, M.; Paksoy, H. O.; Charvat, P. Review on Using Microencapsulated Phase Change Materials (PCM) in Building Applications. *Energy Build.* **2015**, *106*, 134−155.

(7) Du, K.; Calautit, J.; Wang, Z.; Wu, Y.; Liu, H. A Review of the Applications of Phase Change Materials in Cooling, Heating and Power Generation in Different Temperature Ranges. *Appl. Energy* **2018**, *220*, 242−273.

(8) Luzzi, A.; Lovegrove, K.; Filippi, E.; Fricker, H.; Schmitz-goeb, M.; Chandapillai, M.; Kaneff, S. Techno-Economic Analysis of a 10 MWe Solar Thermal Power Plant Using Ammonia-Based Thermochemical Energy Storage. *Fuel Energy Abstr.* **1999**, *40*, 403.

(9) Wentworth, W. *Thermochemical Cycles for Energy Storage: Thermal Decomposition of ZnCO4 Systems*; Final topical report, January 1, 1982−December 31, 1984. No. NREL/TP-253-4279. National Renewable Energy Lab., Golden, CO (United States); Houston University: Texas, USA, 1992.

(10) Ishitobi, H.; Uruma, K.; Takeuchi, M.; Ryu, J.; Kato, Y. Dehydration and Hydration Behavior of Metal-Salt-Modified Materials for Chemical Heat Pumps. *Appl. Therm. Eng.* **2013**, *50*, 1639−1644.

(11) Kumar, A.; Shukla, S. K. A Review on Thermal Energy Storage Unit for Solar Thermal Power Plant Application. *Energy Procedia* **2015**, *74*, 462−469.

(12) Alptekin, E.; Ezan, M. A. Performance Investigations on a Sensible Heat Thermal Energy Storage Tank with a Solar Collector under Variable Climatic Conditions. *Appl. Therm. Eng.* **2020**, *164*, No. 114423.

(13) Olivares, R. I. The Thermal Stability of Molten Nitrite/Nitrates Salt for Solar Thermal Energy Storage in Different Atmospheres. *Sol. Energy* **2012**, *86*, 2576−2583.

(14) Bruch, A.; Fourmigué, J. F.; Couturier, R. Experimental and Numerical Investigation of a Pilot-Scale Thermal Oil Packed Bed Thermal Storage System for CSP Power Plant. *Sol. Energy* **2014**, *105*, 116−125.

(15) Guillot, S.; Faik, A.; Rakhmatullin, A.; Lambert, J.; Veron, E.; Echegut, P.; Bessada, C.; Calvet, N.; Py, X. Corrosion Effects between Molten Salts and Thermal Storage Material for Concentrated Solar Power Plants. *Appl. Energy* **2012**, *94*, 174−181.

(16) Heller, L. *Literature Review on Heat Transfer Fluids and Thermal Energy Storage Systems in CSP Plants*; STERG Report: Stellenbosch, RSA, 2013.

(17) Jemmal, Y.; Zari, N.; Maaroufi, M. Experimental Characterization of Siliceous Rocks to Be Used as Filler Materials for Air-Rock Packed Beds Thermal Energy Storage Systems in Concentrated Solar Power Plants. *Sol. Energy Mater. Sol. Cells* **2017**, *171*, 33−42.

(18) Schmidt, P.; Masse, S.; Laurent, G.; Slodczyk, A.; Le Bourhis, E.; Perrenoud, C.; Livage, J.; Fröhlich, F. Crystallographic and Structural Transformations of Sedimentary Chalcedony in Flint upon Heat Treatment. *J. Archaeol. Sci.* **2012**, *39*, 135−144.

(19) Allen, K. G.; Von Backström, T. W.; Kröger, D. G.; Kisters, A. F. M. Rock Bed Storage for Solar Thermal Power Plants: Rock Characteristics, Suitability, and Availability. *Sol. Energy Mater. Sol. Cells* **2014**, *126*, 170−183.

(20) Hanley, E. J.; Dewitt, D. P.; Roy, R. F. The thermal diffusivity of eight well-characterized rocks for the temperature range 300−1000 K. *Eng. Geol.* **1978**, *12*, 31−47.

(21) Grirate, H.; Agalit, H.; Zari, N.; Elmchaouri, A.; Molina, S.; Couturier, R. Experimental and Numerical Investigation of Potential Filler Materials for Thermal Oil Thermocline Storage. *Sol. Energy* **2016**, *131*, 260−274.

(22) Liu, J.; Yang, J.; Chen, M.; Lei, L.; Wu, Z. Effect of SiO_2, Al_2O_3 on Heat Resistance of Basalt Fiber. *Thermochim. Acta* **2018**, *660*, 56−60.

(23) Liu, J.; Cui, Y.; Yang, J.; Wu, Z. Effect of Basalt Composition and Mineral on High Temperature Melting Process. *J. Yanshan Univ.* **2017**, *41*, 323−328.

(24) Cheng, J. S.; Kang, J. F.; Lou, X. C.; Tang, F. Y.; Liu, K. Effect of Fe_2O_3 and ZrO_2 on the Crystallization Behavior of Glass Ceramics Prepared from Granite. *J. Wuhan Univ. Technol.* **2014**, *36*, 22−25.

(25) Li, B. W.; Deng, L. B.; Zhang, X. F.; Jia, X. L. Structure and Performance of Glass-Ceramics Obtained by Bayan Obo Tailing and Fly Ash. *J. Non-Cryst. Solids* **2013**, *380*, 103−108.

(26) Gan, F. X. *Calculation and Composition Design of Inorganic Glass Physical Properties*; Science and Technology Press: Shanghai, 1981.

(27) Shelby, J. E. *Introduction to Glass Science and Technology*; Royal Society of Chemistry, 2005.

(28) NI, H. Advances and Application in Physicochemical Properties of Silicate Melts. *Chin. Sci. Bull.* **2013**, *58*, 865−890.

(29) Xiao, Z.; Lu, A.; Lu, F. Relationship between Thermal Expansion Coefficient and Composition of R_2O-MO-Al_2O_3-SiO_2 System Glass. *Adv. Mater. Res.* **2006**, *37*, 65−68.

(30) Lubas, M.; Sitarz, M.; Fojud, Z.; Jurga, S. Structure of Multicomponent SiO_2-Al_2O_3-Fe_2O_3-CaO-MgO Glasses for the Preparation of Fibrous Insulating Materials. *J. Mol. Struct.* **2005**, *744*−*747*, 615−619.

(31) Ye, S. Q.; He, F.; Chen, J.; Yang, H.; Liu, X. Q.; Xie, J. L. Effect of Al/Si on Structure and Properties of SiO_2-Al_2O_3-MgO Glass. *J. Wuhan Univ. Technol.* **2017**, *36*, 22−25.

(32) Loutou, M.; Hajjaji, M.; Mansori, M.; Favotto, C.; Hakkou, R. Phosphate Sludge: Thermal Transformation and Use as Lightweight Aggregate Material. *J. Environ. Manage.* **2013**, *130*, 354−360.

(33) Jamshaid, H.; Mishra, R.; Militky, J.; Pechociakova, M.; Noman, M. T. Mechanical, Thermal and Interfacial Properties of Green Composites from Basalt and Hybrid Woven Fabrics. *Fibers Polym.* **2016**, *17*, 1675−1686.

https://dx.doi.org/10.1021/acsomega.0c02773
ACS Omega 2020, 5, 19236−19246

(34) Farmer, V. C.; Palmieri, F. The Characterization of Soil Minerals by Infrared Spectroscopy. In *Soil Components*; Springer: Berlin, Heidelberg, 1975.
(35) Chen, X.; Jiang, J.; Yan, F.; Tian, S.; Li, K. A Novel Low Temperature Vapor Phase Hydrolysis Method for the Production of Nano-Structured Silica Materials Using Silicon Tetrachloride. *RSC Adv.* **2014**, *4*, 8703−8710.
(36) Bigl, S.; Heinz, W.; Kahn, M.; Schoenherr, H.; Cordill, M. J. High-Temperature Characterization of Silicon Dioxide Films with Wafer Curvature. *JOM* **2015**, *67*, 2902−2907.
(37) Nahhas, T.; Py, X.; Sadiki, N.; Gregoire, S. Assessment of Four Main Representative Flint Facies as Alternative Storage Materials for Concentrated Solar Power Plants. *J. Energy Storage* **2019**, *23*, 79−88.
(38) Glover, P. W. J.; Baud, P.; Darot, M.; Zoussi, S.; Leravaleq, S. M.; Reusche, T. α/β Phase Transition in Quartz Monitored Using Acoustic Emissions. *Geophys. J. Int.* **1995**, *120*, 775−782.
(39) Nahhas, T.; Py, X.; Sadiki, N. Experimental Investigation of Basalt Rocks as Storage Material for High-Temperature Concentrated Solar Power Plants. *Renewable Sustainable Energy Rev.* **2019**, *110*, 226−235.
(40) Li, F.; Liu, X. Effect TiO2 of Made of Ash Fly on Crystallization Activation Energy and Index. *MATEC Web Conf.* **2015**, *34*, 2−5.
(41) Ding, Y. F.; Zhang, Y.; Zhang, F. W.; Zhang, D. H.; Li, Z. P. High Temperature Molecular Dynamics Study of Thermal Expansion Properties of Quartz Glass. *Rare Met. Mater. Eng.* **2007**, *36*, 331−333.
(42) Laing, D.; Steinmann, W. D.; Tamme, R.; Richter, C. Solid Media Thermal Storage for Parabolic Trough Power Plants. *Sol. Energy* **2006**, *80*, 1283−1289.
(43) Gil, A.; Medrano, M.; Martorell, I.; Lázaro, A.; Dolado, P.; Zalba, B.; Cabeza, L. F. State of the Art on High Temperature Thermal Energy Storage for Power Generation. Part 1-Concepts, Materials and Modellization. *Renewable Sustainable Energy Rev.* **2010**, *14*, 31−55.
(44) Özrahat, E.; Ünalan, S. Thermal Performance of a Concrete Column as a Sensible Thermal Energy Storage Medium and a Heater. *Renewable Energy* **2017**, *111*, 561−579.
(45) Alcaraz, A.; Montalà, M.; Valderrama, C.; Cortina, J. L.; Akbarzadeh, A.; Farran, A. Increasing the Storage Capacity of a Solar Pond by Using Solar Thermal Collectors: Heat Extraction and Heat Supply Processes Using in-Pond Heat Exchangers. *Sol. Energy* **2018**, *171*, 112−121.
(46) Sarbu, I.; Sebarchievici, C. A Comprehensive Review of Thermal Energy Storage. *Sustainability* **2018**, *10*, No. 191.
(47) Özkahraman, H. T.; Selver, R.; Işk, E. C. Determination of the Thermal Conductivity of Rock from P-Wave Velocity. *Int. J. Rock Mech. Min. Sci.* **2004**, *41*, 703−708.
(48) Stephens, R. B. Low-Temperature Specific Heat and Thermal Conductiviy of Noncrystalline Dielectric Solids. *Phys. Rev. B* **1973**, *8*, 2896−2905.
(49) Fernandez, A. I.; Martnez, M.; Segarra, M.; Martorell, I.; Cabeza, L. F. Selection of Materials with Potential in Sensible Thermal Energy Storage. *Sol. Energy Mater. Sol. Cells* **2010**, *94*, 1723−1729.
(50) Tiskatine, R.; Oaddi, R.; Ait El Cadi, R.; Bazgaou, A.; Bouirden, L.; Aharoune, A.; Ihlal, A. Suitability and Characteristics of Rocks for Sensible Heat Storage in CSP Plants. *Sol. Energy Mater. Sol. Cells* **2017**, *169*, 245−257.
(51) Elouali, A.; Kousksou, T.; El Rhafiki, T.; Hamdaoui, S.; Mahdaoui, M.; Allouhi, A.; Zeraouli, Y. Physical Models for Packed Bed: Sensible Heat Storage Systems. *J. Energy Storage* **2019**, *23*, 69−78.
(52) DRURY, M. J. Thermal Diffusivity of Some Crystalline Rocks. *Geothermics* **1987**, *16*, 105−115.
(53) Höhne, G.; Hemminger, W. F.; Flammersheim, H. J. *Differential Scanning Calorimetry*; Springer Science & Business Media, 2013.

https://dx.doi.org/10.1021/acsomega.0c02773
ACS Omega 2020, 5, 19236−19246